A SCHEME FOR CRACK LOCALIZATION IN COMPOSITE PLATES COMBINING THE EXTENDED AND THE WAVE FINITE ELEMENT METHODS

Konstantinos D. Sfoungaris[1], Dimitrios G. Chronopoulos[1] and Savvas P. Triantafyllou[2]

[1]Composites Group, Faculty of Engineering, The University of Nottingham, NG7 2RD, United Kingdom
Email: Konstantinos.sfoungaris@nottingham.ac.uk
[2]Centre for Structural Engineering and Informatics, Faculty of Engineering, The University Of Nottingham, NG7 2RD, United Kingdom

Keywords: Structural health monitoring, Wave finite element method, Extended finite element method, Non-destructive testing

Abstract
Inspection of structures comprising composite materials is a time-consuming and expensive, yet necessary process. Acoustic methods are common ground in non-destructive testing, utilizing wave reflection and transmission properties to localize and identify defects. In this work, a hybrid eXtended-Wave Finite Element method is employed to study those properties on a damaged waveguide. The implementation is discussed and numerical results are provided. The proposed model's advantage is the reduction of computational cost for both the vibrational and the remeshing aspect.

1. Introduction

Usage of composite materials has expanded in recent years, especially in the aerospace and automotive industry. Costs for inspection however, have been estimated to reach 27% of the structure's life-cycle [1]; the field of *Structural Health Monitoring (SHM)* has thus become relevant, aiming at developing methods for *Non-Destructive Testing* of structures to detect and assess operation-induced defects. Towards that goal, a variety of methods have been conceived and implemented [2]; among these, the *vibration-based* ones are dominating the field [3], [4]. This class of methods consists of emitting a vibration that travels through the structure and interacts with flaws; receiving the altered signal yields information about the state of the structure or the existence and characteristics of any flaws [5]. Implementing knowledge of the underlying physics towards modelling the governing phenomena contributes to further understanding thereof. Computational methods—predominantly finite elements—are widely implemented in this context. Demand for higher efficiency had led to the development of more specialized tools, such as the Wave Finite Element (WFE) and the eXtended Finite Element Method (XFEM).

The *Wave Finite Element* method has been well-established as means of analysing the vibrational behaviour of a structure. It is most suited to accommodate for guided waves in long structures and takes advantage of a structure's periodicity, vastly reducing the computational cost, especially in higher frequencies. The method was developed by Zhong and Williams [6]. In [7] the *reflection* and *transmission* of waves between *waveguides* of different directions, joined by a *coupling element* is investigated and validated. In [8] the *Diffusion Matrix prediction Model* is further elaborated upon and the reflection, transmission and intermodal conversion of waves through notched waveguides, is

investigated. Further works examining and validating different configurations are Renno and Mace [9], Mitrou et al. [10], whereas several extensions exist, such as [11] which examines nonlinear behaviour along with the generation of harmonics.

XFEM was initially introduced in a fracture mechanics context, to improve convergence properties of finite element solutions for cracks by incorporating a priori knowledge of the solution behaviour, through a Partition of Unity framework. The introduction of a Heaviside type enrichment for nodes whose support is cut by the crack, allowed free separation, leading to a complete mesh-free representation of cracks. The XFEM's mesh-free capabilities wire first implemented in a SHM context in Rabinovich et al. [12], [13] taking advantage of the mesh-free representation of cracks to eliminate need for remeshing at each iteration of the forward problem. Several papers followed. [12]–[16] implemented *Genetic Algorithms* to detect and identify one or multiple flaws. In [17] and [18] optimization strategies involving identification at multiple scales are adopted. Nanthakumar et al. [19], [20] solved the coupled equations to identify cracks in piezoelectric materials. Yan et al. [21], Sun et al. [22] used *Bayesian inference* methods in a stochastic approach taking into account sensor noise.

This paper investigates the reflection, transmission and conversion of waves through a crack. The *WFE* and *XFEM* are combined, aiming at reducing the computational cost for higher frequency vibrations, along with the need for complex meshing, re-meshing and tying approaches such as the *mortar method* implemented in i.e. [8]. In Section 2 the formulation for the *WFE* and the *coupling element* problem are given. Numerical results and discussion thereof are presented in Section 3.

2. The WFE and the XFEM

2.1 The WFE

An infinitely long domain Ω of constant section, as depicted in Figure 1, is considered. The domain contains a crack. The partition of the geometry into $\Omega_1 \cup \Omega_c \cup \Omega_2$ with bounds $\Gamma_1^R \equiv \Gamma_c^L$, $\Gamma_2^L \equiv \Gamma_c^R$ is possible. It holds that waves propagate uniformly through $\Omega \setminus \Omega_c$.

2.1.1 1-Dimensional wave propagation in an infinite waveguide

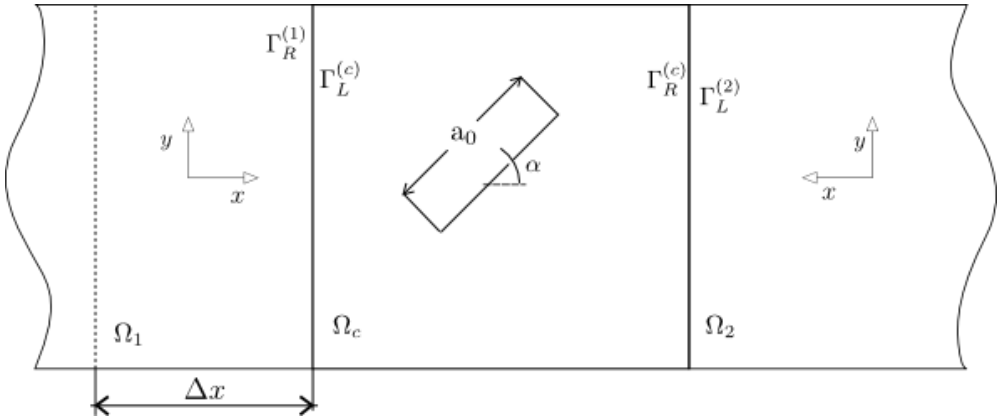

Figure 1. Waveguide partitioned in propagating and cracked substructures

For a wave travelling inside Ω_1, Ω_2 the displacements may be given according to Bloch's theorem [6]:

$$u(x) = u_0 \mathrm{e}^{-\mathrm{i}kx} \tag{1}$$

Following a finite element discretization and obtaining the *stiffness* K and *mass* M matrices, along with the *force vector*, the following equation is established:

$$\begin{bmatrix} \mathrm{D}_{LL} & \mathrm{D}_{LR} & \mathrm{D}_{LI} \\ \mathrm{D}_{RL} & \mathrm{D}_{RR} & \mathrm{D}_{RI} \\ \mathrm{D}_{IL} & \mathrm{D}_{IR} & \mathrm{D}_{RR} \end{bmatrix} \begin{bmatrix} \mathrm{q}_L \\ \mathrm{q}_R \\ \mathrm{q}_I \end{bmatrix} = \begin{bmatrix} \mathrm{f}_L \\ \mathrm{f}_R \\ 0 \end{bmatrix} \tag{2}$$

With $\mathrm{D} = (1+\mathrm{i}\eta\omega)\,\mathrm{K}+\omega^2\mathrm{M}$ the *dynamic stiffness matrix*, where η denotes the damping coefficient and ω the angular frequency. It is then possible to write:

$$\mathrm{T}\begin{bmatrix} \mathrm{q}_L \\ \mathrm{f}_L \end{bmatrix} = \lambda \begin{bmatrix} \mathrm{q}_R \\ \mathrm{f}_R \end{bmatrix} \tag{3}$$

with T the *transfer matrix* and $\lambda = \mathrm{e}^{-\mathrm{i}kx}$. The *transfer matrix* is shown to be *symplectic* [6], [7] and, as such, eigenvalues appear in reciprocal pairs, denoting left and right-travelling waves: $\lambda_j^+ = 1/\lambda_{j+1}^-$. A positive travelling wavemode fulfils the equation:

$$\begin{aligned} \left|\lambda_j^+\right| &\leq 1 \\ \mathfrak{Re}\left\{\mathrm{i}\omega \mathrm{f}_L^{\mathrm{T}} \mathrm{q}_L\right\} &< 0, \text{ if } \left|\lambda_j^+\right| = 1 \end{aligned} \tag{4}$$

Furthermore, the *eigenvectors* of Eq. 3 can be partitioned into *left-travelling* and *right-travelling* and *displacement* and *force* part. This is written as:

$$\Phi_j = \begin{bmatrix} \begin{Bmatrix} \Phi_q \\ \Phi_f \end{Bmatrix}^+ & \begin{Bmatrix} \Phi_q \\ \Phi_f \end{Bmatrix}^- \end{bmatrix} \tag{5}$$

Last, by obtaining the *left eigenvectors* it is possible to make the following normalization:

$$\boldsymbol{\Psi\Phi} = \mathbf{I} \tag{6}$$

with **I** the unit matrix.

2.1.2. The coupling element problem

Considering the stiffness matrix of the coupling element Ω_c and following a *Guyan reduction* on L, R [7], one obtains:

$$\begin{bmatrix} \mathrm{D}_{LL} & \mathrm{D}_{LR} \\ \mathrm{D}_{RL} & \mathrm{D}_{RR} \end{bmatrix} \begin{bmatrix} \mathrm{q}_L \\ \mathrm{q}_R \end{bmatrix} = \begin{bmatrix} \mathrm{f}_L \\ \mathrm{f}_R \end{bmatrix} \tag{7}$$

It is possible to expand the forces and displacements cast on ${\Gamma_L}^{(c)}$, ${\Gamma_R}^{(c)}$ from ${\Gamma_R}^{(1)}$, ${\Gamma_L}^{(2)}$ as the sum of series of eigenmodes such that:

$$\mathrm{q}_{\Gamma_i} = \sum_j \Phi_{qj}^{(i)}\, \mathrm{Q}_j^{(i)} \tag{8}$$

with $\mathrm{Q}_j^{(i)}$ the amplitude of j^{th} mode. Subsequently displacement and force vectors can be written in matrix form as:

$$\begin{aligned} \mathrm{q} &= [\Phi_q^+ \quad \Phi_q^-][\mathrm{Q}^+ \quad \mathrm{Q}^-]^{\mathrm{T}} \\ \mathrm{f} &= [\Phi_f^+ \quad \Phi_f^-][\mathrm{Q}^+ \quad \mathrm{Q}^-]^{\mathrm{T}} \end{aligned} \tag{9}$$

The eigenvectors are further regrouped as:

$$\widetilde{\Phi}_k{}^{\pm} = \begin{bmatrix} \Phi_k^{\pm(1)} & 0 \\ 0 & \Phi_k^{\pm(2)} \end{bmatrix} \tag{10}$$

where k stands for q or f, for displacement or force part of the eigenvector, as displayed in Eq. 5. Also $\Phi_k^{\pm(i)}$ expresses the positive/negative travelling wavemode of substructure $i = 1,2$. Since the substructures are *opposite* in the sense that a positive-travelling wave in Ω_1 is negative-travelling in Ω_2, the two are connected via the relation $\Phi_k^{\pm(1)} = \mathrm{R}\Phi_k^{\pm(2)}$ with R a rotation matrix setting $x^{(1)} =$

$-x^{(2)}$, $y^{(1)} = y^{(2)}$. Then, substituting Equations 9, 10, Eq. 7 for the *coupling element* can be rewritten as:

$$\begin{bmatrix} \mathrm{D}\,\widetilde{\Phi}_q^- - \widetilde{\Phi}_f^- & \mathrm{D}\,\widetilde{\Phi}_q^+ - \widetilde{\Phi}_f^+ \end{bmatrix} \begin{Bmatrix} \mathrm{Q}^{+(1)} \\ \mathrm{Q}^{+(2)} \\ \mathrm{Q}^{-(1)} \\ \mathrm{Q}^{-(2)} \end{Bmatrix} = 0 \tag{11}$$

$$\begin{Bmatrix} \mathrm{Q}^{-(1)} \\ \mathrm{Q}^{-(2)} \end{Bmatrix} = \mathrm{s} \begin{Bmatrix} \mathrm{Q}^{+(1)} \\ \mathrm{Q}^{+(2)} \end{Bmatrix} \tag{12}$$

$$\mathrm{s} = \left[\mathrm{D}\,\widetilde{\Phi}_q^- - \widetilde{\Phi}_f^-\right]^{-1} \left[\mathrm{D}\,\widetilde{\Phi}_q^+ - \widetilde{\Phi}_f^+\right] \tag{13}$$

The *scattering matrix* s is defined by Eq. 12 which, combined with Eq. 11 reaches the form of Eq. 13. As a reduced basis of eigenvectors is retained in general, *pseudo-inversion* is employed in Eq. 13.

2.2 The XFEM

Considering a domain Ω bounded by $\Gamma = \Gamma_u \cup \Gamma_t$, with $\Gamma_u \cap \Gamma_t = \emptyset$, containing a crack Γ_c the equations of equilibrium read:

$$\begin{aligned} \mathrm{div}\sigma - \rho\ddot{\mathrm{u}} &= 0 \\ \sigma &= \mathrm{C}{:}\varepsilon \\ \varepsilon &= \nabla^{sym}\mathrm{u} \\ \mathrm{u} &= \mathrm{u}_0 \text{ on } \Gamma_u \\ \sigma{\cdot}\mathrm{n} &= \mathrm{t} \text{ on } \Gamma_t \\ \sigma{\cdot}\mathrm{n} &= 0 \text{ on } \Gamma_c \end{aligned} \tag{14}$$

In Eq. 14, σ describes the Cauchy stress tensor, ε the strain tensor, u the displacement field, C is Hooke's tensor and n the outward normal vector. Following a finite element discretisation, the displacement field can be expressed as:

$$\mathrm{u}(x) = \sum_{i\in\mathcal{I}} N_i(x)\mathrm{u}_i + \sum_{i\in\mathcal{J}} N_i(x)H_i\mathrm{b}_i + \sum_{i\in\mathcal{K}} N_i(x)\sum_{k=1}^{n_k} F_{ik}\mathrm{a}_{ik} \tag{15}$$

where N_i are the finite element shape functions, with $N_i(x_j) = 1\ if\ i = j, 0\ else$ the Kronecker delta property and $\sum_{i\in\mathcal{I}} N_i(x) = 1\ \forall x \in \Omega$ the *Partition of Unity* property. The set $\mathcal{I}$ represents all the nodes in Ω. The set $\mathcal{J}$ represents the nodes whose support is cut by the crack, which are enriched by a Heaviside type function. The set $\mathcal{K}$ contains all the nodes whose behaviour is assumed to be influenced from the near-tip behaviour, and are thus enriched with the function kernel in Equation 16b; n_k is the number of enrichment terms employed. For most cases, including the present, four functions are retained. The nodes $\mathcal{K}$ are chosen so that they lie sufficiently close to the crack tip.

$$H_i = [H(\phi(x)) - H(\phi(x_i))] \tag{16a}$$

$$F = \{\sqrt{r}cos\left(\frac{\theta}{2}\right), \sqrt{r}sin\left(\frac{\theta}{2}\right), \sqrt{r}cos\left(\frac{\theta}{2}\right)sin(\theta), \sqrt{r}cos\left(\frac{\theta}{2}\right)cos(\theta)\} \tag{16b}$$

and $F_i = F(x) - F(x_i)$. The crack is represented by the *level set functions*. Those are defined as:

$$\phi(x) = \min_{x_c\in\Gamma_c}(\|x - x_c\|)\mathrm{sign}(n \cdot (x - x_c)) \tag{17}$$

$\psi(x)$ is a signed distance function normal to $\phi(x)$ such that $\psi(x) = 0$ at the crack front (18)

Then r, θ can be expressed as:

$$r = \sqrt{\phi^2 + \psi^2}$$
$$\theta = \arctan(\frac{\phi}{\psi}) \quad (19)$$

3. Wave Reflection and Transmission through a cracked waveguide

A thin aluminium bar of infinite length is considered. The material is aluminium, the width is H=15mm and the thickness t=2mm. A plane stress assumption is used and only the in plane motion and stress are taken into account. The crack, of length a_0 runs through the thickness and is located mid-width, inclined by an angle α. The geometry can be broken down as in Figure 1. Following the Equations 1-6 a set of waves is produced for a frequency span of $f = 10^3 \sim 10^5\ Hz$. Two propagating wave modes are generated, *longitudinal* and *bending*. The dispersion curve is displayed in Figure 1. Comparing the wavenumbers to the analytical relations for an Euler-Bernoulli beam, good agreement is shown at lower frequencies.

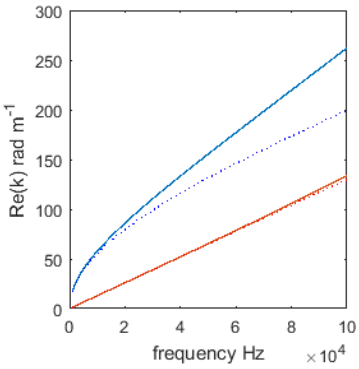

Figure 2. Dispersion curves for *bending* (blue) and *membrane* (red) wavemode. Lines denote: (—) WFE, (···) Euler-Bernoulli analytic relations.

Regarding the wave reflection and transmission, observing at Figures 3, 4, the following remarks can be made about the crack-wave interaction.

First, the waveguide responds differently under different frequency excitations. In graphs (a) and (c) the reflection and transmission coefficients respectively for a bending wave are depicted; in (f) and (h) respective for membrane. For lower frequencies, the waves do not interact with the crack. As the frequency increases, a bigger proportion of a given wave's energy is reflected. This can be attributed to the need for the wavelength to be pertinent to the defect size. In general, the shorter the wave length, the greater the resolution achieved. Furthermore, in Fig. 3a it is shown that the reflection coefficient is maximized at 50000 Hz, for larger cracks and regresses for higher frequencies. This is due to waves reaching an optimal resonance frequency; for higher frequencies, waves of smaller length may bypass or be converted at the flaw.

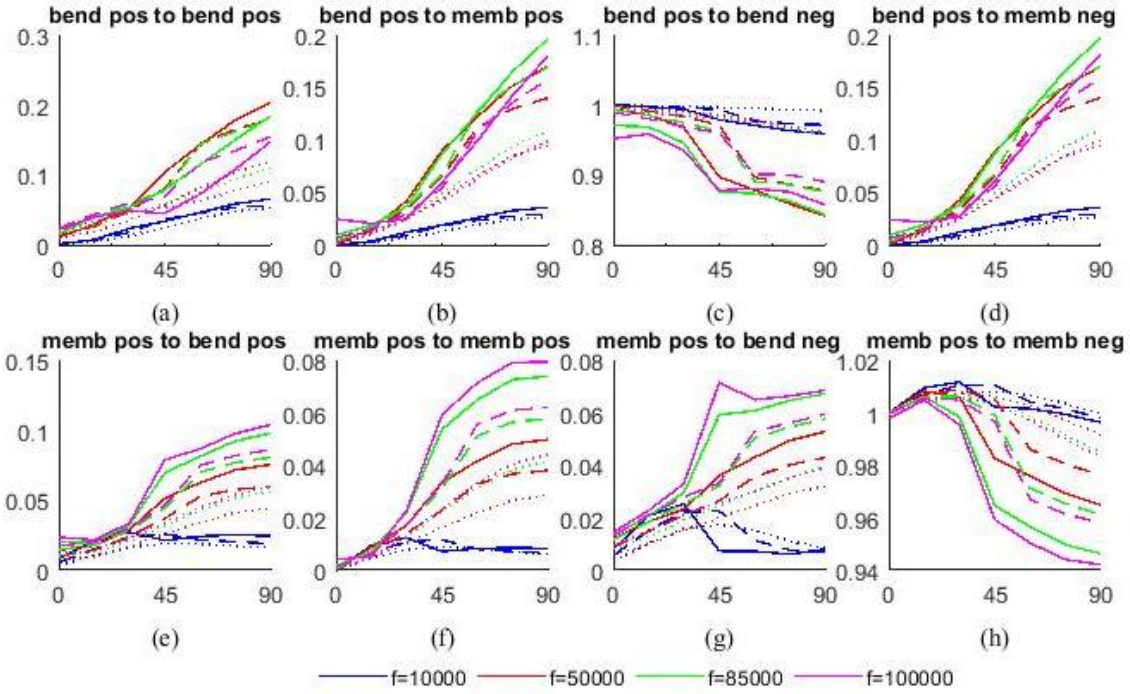

Figure 3. *Reflection-Transmission Coefficients* againist crack angle for selected frequencies. Different crack sizes are represented with lines: continuous (—) H/3, dashed (---) H/4, dotted (···) H/5.

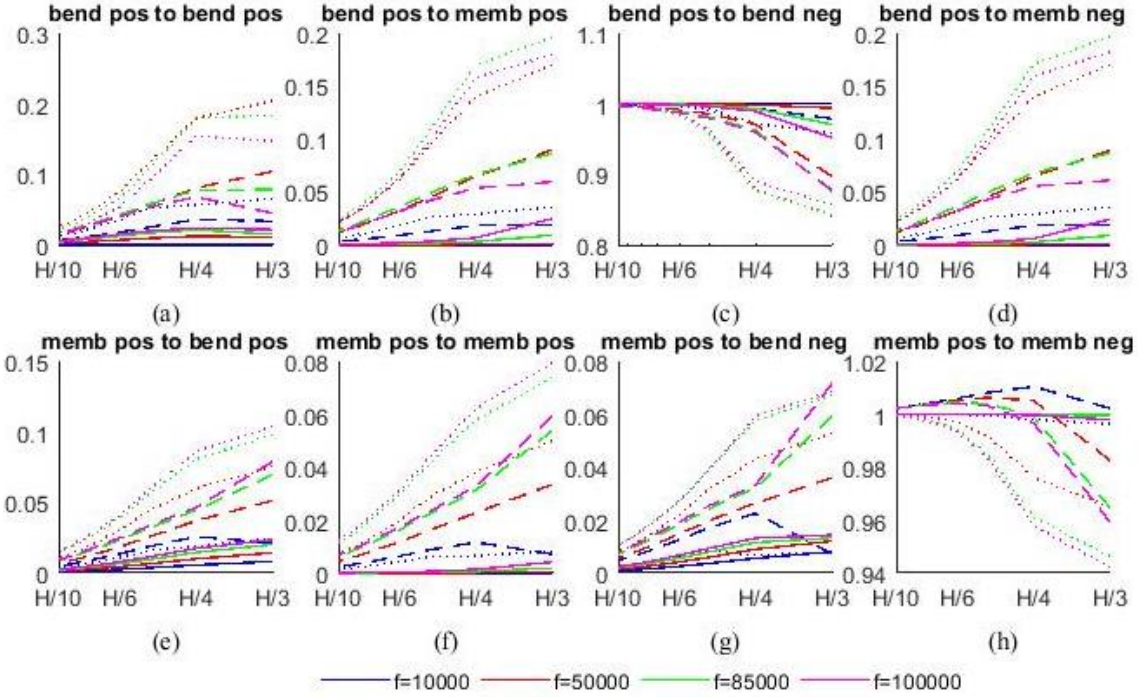

Figure 3. *Reflection-Transmission Coefficients* againist crack length for selected frequencies. Different angles are represented with lines: continuous (—) 0°, dashed (---) 45°, dotted (···) 90°.

4. Conclusions

The reflection and transmission of waves on a cracked waveguide was investigated by combining the WFE for the modelling of propagating waves and the XFEM for modelling the crack. Very little engagement was required, both computationally and with respect to the operator, as XFEM facilitates the crack parametrization and eliminates the need for mesh tying operations is eliminated, as the need for complicated mesh strategies due to defect geometry are also eliminated, thus leaving nothing to prevent substructure-waveguide meshes conforming.

References

[1] S. S. Kessler, S. M. Spearing, and C. Soutis, "Damage detection in composite materials using Lamb wave methods," *Smart Mater. Struct.*, vol. 11, no. 2, pp. 269–278, Apr. 2002.

[2] D. M. Amafabia, D. Montalvão, O. David-West, and G. Haritos, "A Review of Structural Health Monitoring Techniques as Applied to Composite Structures.," *SDHM Struct. Durab. Heal. Monit.*, vol. 11, no. 2, pp. 91–147, 2018.

[3] A. J. Croxford, P. D. Wilcox, B. W. Drinkwater, and G. Konstantinidis, "Strategies for guided-wave structural health monitoring," *Proc. R. Soc. A Math. Phys. Eng. Sci.*, vol. 463, no. 2087, pp. 2961–2981, Nov. 2007.

[4] R. Guan, Y. Lu, W. Duan, and X. Wang, "Guided waves for damage identification in pipeline structures: A review," *Struct. Control Heal. Monit.*, vol. 24, no. 11, p. e2007, Nov. 2017.

[5] Z. Su, L. Ye, and Y. Lu, "Guided Lamb waves for identification of damage in composite structures: A review," *J. Sound Vib.*, vol. 295, no. 3–5, pp. 753–780, 2006.

[6] W. X. Zhong and F. W. Williams, "On the direct solution of wave propagation for repetitive structures," *J. Sound Vib.*, vol. 181, no. 3, pp. 485–501, 1995.

[7] J.-M. Mencik and M. N. Ichchou, "Multi-mode propagation and diffusion in structures through finite elements," *Eur. J. Mech. - A/Solids*, vol. 24, no. 5, pp. 877–898, Sep. 2005.

[8] M. N. Ichchou, J.-M. Mencik, and W. Zhou, "Wave finite elements for low and mid-frequency description of coupled structures with damage," *Comput. Methods Appl. Mech. Eng.*, vol. 198, no. 15–16, pp. 1311–1326, 2009.

[9] J. M. Renno and B. R. Mace, "Calculation of reflection and transmission coefficients of joints using a hybrid finite element/wave and finite element approach," *J. Sound Vib.*, vol. 332, no. 9, pp. 2149–2164, 2013.

[10] G. Mitrou, N. Ferguson, and J. Renno, "Wave transmission through two-dimensional structures by the hybrid FE/WFE approach," *J. Sound Vib.*, vol. 389, pp. 484–501, Feb. 2017.

[11] D. Chronopoulos, "Calculation of guided wave interaction with nonlinearities and generation of harmonics in composite structures through a wave finite element method," *Compos. Struct.*, vol. 186, pp. 375–384, Feb. 2018.

[12] D. Rabinovich, D. Givoli, and S. Vigdergauz, "XFEM-based crack detection scheme using a genetic algorithm," *Int. J. Numer. Methods Eng.*, vol. 71, no. 9, pp. 1051–1080, Aug. 2007.

[13] D. Rabinovich, D. Givoli, and S. Vigdergauz, "Crack identification by 'arrival time' using XFEM and a genetic algorithm," *Int. J. Numer. Methods Eng.*, vol. 77, no. 3, pp. 337–359, Jan. 2009.

[14] H. Waisman, E. Chatzi, and A. W. Smyth, "Detection and quantification of flaws in structures by the extended finite element method and genetic algorithms," *Int. J. Numer. Methods Eng.*, vol. 82, no. 3, pp. 303–328, 2009.

[15] E. N. Chatzi, B. Hiriyur, H. Waisman, and A. W. Smyth, “Experimental application and enhancement of the XFEM–GA algorithm for the detection of flaws in structures,” *Comput. Struct.*, vol. 89, no. 7–8, pp. 556–570, Apr. 2011.

[16] K. Agathos, E. Chatzi, · Stéphane, and P. A. Bordas, “Multiple crack detection in 3D using a stable XFEM and global optimization.”

[17] C. Ma, T. Yu, L. Van Lich, and T. Quoc Bui, “An effective computational approach based on XFEM and a novel three-step detection algorithm for multiple complex flaw clusters,” *Comput. Struct.*, vol. 193, pp. 207–225, Dec. 2017.

[18] H. Sun, H. Waisman, and R. Betti, “Nondestructive identification of multiple flaws using XFEM and a topologically adapting artificial bee colony algorithm,” *Int. J. Numer. Methods Eng.*, vol. 95, no. 10, pp. 871–900, Sep. 2013.

[19] S. S. Nanthakumar, T. Lahmer, and T. Rabczuk, “Detection of multiple flaws in piezoelectric structures using XFEM and level sets,” *Comput. Methods Appl. Mech. Eng.*, vol. 275, pp. 98–112, Jun. 2014.

[20] S. S. Nanthakumar, T. Lahmer, and T. Rabczuk, “Detection of multiple flaws in piezoelectric structures using XFEM and level sets,” *Int. J. Numer. Methods Eng.*, vol. 105, no. 12, pp. 960–960, Mar. 2016.

[21] G. Yan, H. Sun, and H. Waisman, “A guided Bayesian inference approach for detection of multiple flaws in structures using the extended finite element method,” *Comput. Struct.*, vol. 152, pp. 27–44, May 2015.

[22] J. He, J. Yang, Y. Wang, H. Waisman, and W. Zhang, “Probabilistic Model Updating for Sizing of Hole-Edge Crack Using Fiber Bragg Grating Sensors and the High-Order Extended Finite Element Method,” *Sensors*, vol. 16, no. 11, p. 1956, Nov. 2016.